Porous, Platinum Nanoparticle-Adsorbed Carbon Nanotube Yarns for Efficient Fiber Solar Cells

Sen Zhang,[†,#] Chunyan Ji,[‡,#] Zuqiang Bian,[§] Pingrong Yu,[†] Luhui Zhang,[‡] Dianyi Liu,[§] Enzheng Shi,[‡] Yuanyuan Shang,[‡] Haitao Peng,[†] Qiao Cheng,[†] Dong Wang,[†,*] Chunhui Huang,[§] and Anyuan Cao[‡,*]

[†]Department of Energy and Resources Engineering, College of Engineering, Peking University, Beijing 100871, People's Republic of China, [‡]Department of Materials Science and Engineering, College of Engineering, Peking University, Beijing 100871, People's Republic of China, and [§]Beijing National Laboratory for Molecular Science, State Key Laboratory of Rare Earth Materials and Applications, College of Chemistry and Molecular Engineering, Peking University, Beijing 100871, People's Republic of China. [#]These authors contributed equally to this work.

ABSTRACT Pt is a classical catalyst that has been extensively used in fuel cell and solar cell electrodes, owing to its high catalytic activity, good conductivity, and stability. In conventional fiber-shaped solar cells, solid Pt wires are usually adopted as the electrode material. Here, we report a Pt nanoparticle-adsorbed carbon nanotube yarn made by solution adsorption and yarn spinning processes, with uniformly dispersed Pt nanoparticles through the porous nanotube network. We have fabricated TiO_2-based dye-sensitized fiber solar cells with a Pt–nanotube hybrid yarn as counter electrode and achieved a power conversion efficiency of 4.85% under standard illumination (AM1.5, 100 mW/cm^2), comparable to the same type of fiber cells with a Pt wire electrode (4.23%). Adsorption of Pt nanoparticles within a porous nanotube yarn results in enhanced Pt–electrolyte interfacial area and significantly reduced charge-transfer resistance across the electrolyte interface, compared to a pure nanotube yarn or Pt wire. Our porous Pt–nanotube hybrid yarns have the potential to reduce the use of noble metals, lower the device weight, and improve the solar cell efficiency.

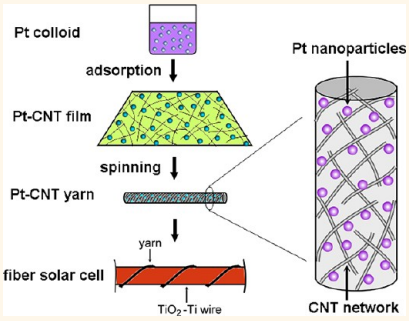

KEYWORDS: fiber solar cell · Pt nanoparticle · carbon nanotube yarn · adsorption · hybrid

Fiber solar cells (FSCs) represent typical flexible electronics for solar energy harvesting. With integration, FSC-based power-supply fabric can be applied to irregular objects or embedded into portable devices and clothes. To date, most reported FSCs with relatively high power conversion efficiencies (>4%) adopt Pt wires as the counter electrode, which serves as a charge carrier collection and transport path.[1−5] Pt is the most widely used electrode material for electrochemical energy conversion devices such as dye-sensitized solar cells and hydrogen fuel cells, owing to its high catalytic activity, good electrical conductivity, and stability in various chemicals.[6−9] To lower the manufacturing cost, other inexpensive electrode materials have been explored recently, including conventional metal wires (*e.g.*, stainless steel, Ti), semiconducting wires, and carbon fibers.[10−15] In general, those materials necessitate a surface coating such as a metal film, conducting polymer layer, or paste of carbon ink in order to improve the electrode conductivity and catalytic activity. For the FSCs using carbon fiber electrodes, a thin layer of Pt film or particles was deposited onto the fiber surface to improve the FSC performance, yet the Pt particles tend to aggregate on the smooth fiber surface and the brittle fiber is not ideal for making flexible devices.[12−14] Due to such limitations, most FSCs made by alternative counter electrodes generally show lower level efficiencies (<3%) compared to Pt wire.[12,14,15]

Another strategy is to deposit fine Pt nanoparticles onto a porous membrane such as carbon nanotube (CNT) arrays or networks, as demonstrated in planar structure dye-sensitized solar cells as well as in fuel cells.[7−9,16−18] This could reduce the amount of Pt in use and further improve its activity by controlling the crystal structure and particle size.[16−18] With appropriate assembly into a one-dimensional structure, Pt nanoparticles may also serve as counter electrodes for FSCs to replace solid Pt wires. Although nanoparticles in powder form are difficult to convert to one-dimensional wire-like structures, some particles (*e.g.*, Ti, TiO_2, SiO_2) have been combined with CNT sheets and subsequently spun into yarns, sustaining functional particles.[19] In this article, we adsorbed Pt nanoparticles onto a freestanding CNT spiderweb and then spun the hybrid film into a thin, flexible yarn with

* Address correspondence to wangdong@coe.pku.edu.cn, anyuan@pku.edu.cn.

Received for review May 22, 2012 and accepted August 3, 2012.

Published online August 03, 2012
10.1021/nn3022553

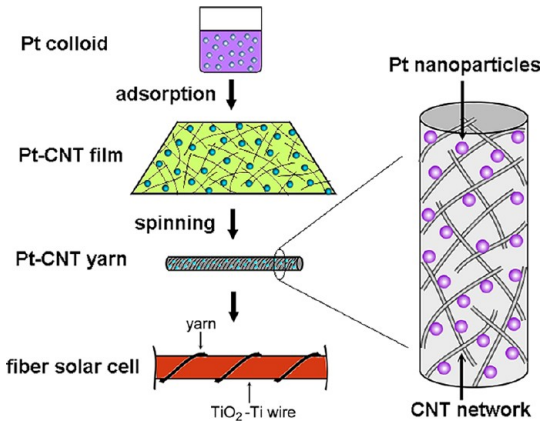

Figure 1. Illustration of the preparation processes of Pt-adsorbed hybrid yarns and application as counter electrodes for fiber solar cells. A colloid containing 2−3 nm Pt nanoparticles was made, and then the nanoparticles were adsorbed onto a spread CNT film like a fine fishnet. The Pt-loaded CNT film was then spun into a one-dimensional thin yarn consisting of a porous CNT network and dispersed Pt nanoparticles. Finally, the Pt−CNT yarn was twisted around a TiO_2−Ti primary electrode to make the fiber solar cell.

controlled particle loading. The CNT yarning process not only transfers Pt nanoparticles into an integral one-dimensional form but also helps maintain a highly porous structure and uniform dispersion of nanoparticles throughout the entire yarn, both of which are important factors for making electrodes. Furthermore, the interconnected CNTs within the yarn provide a necessary charge carrier transport path and mechanical robustness and flexibility as a support structure for Pt nanoparticles. Applied as counter electrodes for FSCs, our porous Pt-loaded CNT yarns show power conversion efficiencies up to 4.85%, comparable with that of solid Pt wires.

RESULTS AND DISCUSSION

The processes of making Pt−CNT hybrid yarns and fabrication of FSCs involve the following steps, as illustrated in Figure 1. First, a Pt colloid with particle diameters of 2−3 nm was synthesized by a solution process using H_2PtCl_6 as precursor, as described previously.[20] On the other hand, freestanding films or spiderwebs of single-walled nanotubes with sizes up to 100 cm^2 produced by chemical vapor deposition (CVD) by our group were used to support Pt nanoparticles and spinning.[21] Then, a piece of CNT film was immersed into the colloid for 24 h to adsorb nanoparticles physically with controlled loading. After that, the Pt-attached CNT film was twist-spun into yarns with controlled diameter and length by small electric motors (see Methods for details). At the same time, TiO_2 nanotube arrays etched on a Ti wire were prepared by electro-anodization to serve as primary electrodes for constructing FSCs. Finally, CNT yarns without (as control sample) or with Pt nanoparticles were twisted around the TiO_2−Ti wire as counter electrodes, and the device was infiltrated by liquid electrolyte for solar cell testing.

We first studied the performance of a pure CNT yarn without Pt nanoparticles when it acts as an FSC electrode. Figure 2a shows the scanning electron microscopy (SEM) image of a neat CNT yarn with a uniform diameter of 20 μm and length of several centimeters. The helical traces on the yarn surface indicate that it was made from a flat film by spinning. A close view shows that it consists of highly pure CNT bundles interconnected and twisted together (Figure 2b,c). The spacing between CNTs constitutes numerous nanoscale pores inside the yarn, and this highly porous structure is favorable for attaching nanoparticles that would be accessible by liquid electrolyte through infiltration during solar cell assembly. Raman characterization reveals radial breathing mode peaks in the region of 100 to 400 cm^{-1} and a very low disorder band, meaning that the yarn is composed of single-walled or double-walled nanotubes with diameters in the range of 1.2 to 2 nm (Supporting Information, Figure S1). A CNT yarn with 60 μm diameter was twisted periodically around a dye-sensitized TiO_2−Ti primary electrode in a conformal way at a pitch of 3 mm to serve as the counter electrode (Figure 2d). At the interface between the primary and counter electrodes, the CNT yarn is overlapped on the top portion of the TiO_2 nanotube arrays, resulting in a close contact (Figure 2e). After electrolyte infiltration into both the pores of the TiO_2 nanotubes and the CNT yarn, the FSCs are ready for device measurement.

We have measured the anode current density (J) *versus* voltage (V) characteristics of the FSCs with a pure CNT yarn electrode under standard illumination conditions (AM 1.5, 100 mW/cm^2). The illuminated fiber length of each cell is maintained as 0.5 cm. A series of $J-V$ curves for CNT yarns with different diameters are summarized in Figure 2f, showing considerable shift of output current and voltage depending on the yarn diameter. When the yarn diameter increases from 20 to 90 μm, we observe a consistent increase of short-circuit current density (J_{sc}) from 5.22 to 13.52 mA/cm^2, and cell efficiency (η) from 0.49% to 3.38% (Figure 2g). However, the efficiency drops to 2.00% for a larger yarn diameter of 130 μm. It shows that the maximum efficiency is obtained from CNT yarns with diameters around 90 μm. In optimized configuration, the cell also has a reasonable fill factor (FF) of 50% and open-circuit voltage (V_{oc}) of 0.5 V. These results indicate that even without Pt nanoparticles a CNT yarn itself can serve as the counter electrode. It has been reported that single-walled nanotube films are electrochemically active for redox reactions in dye-sensitized solar cells, and the structural defects on the nanotubes form main catalytic sites.[22] The number of catalytic sites available in a yarn is directly related to the yarn size, and the measured catalytic activity shows some dependence

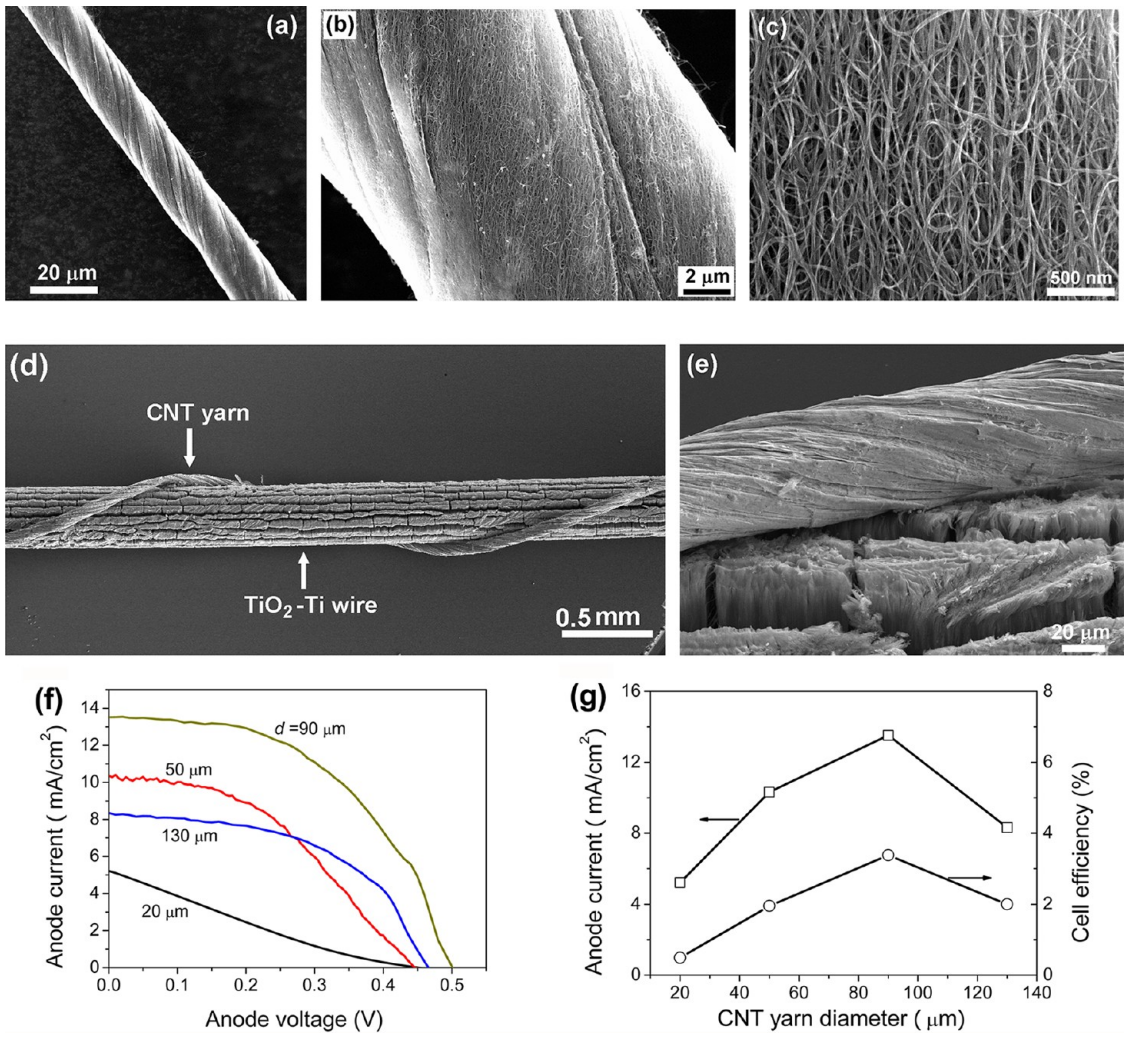

Figure 2. Fiber solar cells with pure CNT yarn electrodes. (a) SEM image of a 20 μm diameter CNT yarn spun from a thin film. (b) Enlarged view of the yarn. (c) Close view of the carbon nanotubes contained in the yarn forming a porous network. (d) SEM image of a 60 μm diameter CNT yarn (as counter electrode) twisted around a TiO_2−Ti primary electrode. (e) Enlarge view showing the yarn twisted around the top surface of the vertical TiO_2 arrays. (f) Anode current density *versus* voltage curves of FSCs with different diameter (*d*) CNT yarns as electrodes. (g) Plots of the anode current densities and cell efficiencies depending on the yarn diameter.

on yarn diameter (described later). In addition, the electrical resistance decreases with thicker yarns; for the yarns with diameters of 20 to 90 μm, the conductivity changes in the range of 100 to 1000 S/cm. Smaller diameter CNT yarns are more flexible and can be readily twisted around the primary electrode to form good contact with TiO_2 (Figure 2d). A combination of the above factors leads to the observed relationship between FSC performance and the yarn diameter.

Previous reports on nanoparticle−CNT hybrid systems offer a promising way to attach active particles on CNTs, and here we introduced Pt nanoparticles into a porous CNT yarn in order to create effective catalytic sites and further improve the solar cell performance. We started from a clean CNT film consisting of a network of single-walled and double-walled nanotubes after purification by hydroxide and HCl (Figure 3a). This film was immersed into a Pt colloid for 24 h to allow Pt nanoparticles to directly adsorb onto the CNT surface without using molecular mediators. Transmission electron microscopy (TEM) images show uniform Pt nanoparticles adsorbed throughout the CNT network with a weight percentage of 87.7 wt % (Figure 3b,c). The Pt loading on the CNT surfaces can be tuned by the initial colloid concentration and maintains a uniform distribution at higher loadings (Figure S2). High-resolution TEM images of individual Pt nanoparticles clearly reveal a lattice parameter of 2.27 Å, corresponding to the distance between (111) crystal faces (inset of Figure 3c). We also performed energy dispersive X-ray (EDX) spectroscopy analysis on the hybrid film, which shows characteristic peaks corresponding to Pt element (Figure S3). TEM and EDX results confirm that we have obtained Pt−-CNT hybrids with a uniform distribution and controlled nanoparticle loadings.

Because Pt nanoparticles were attached to the CNT film before twisting into a yarn, our Pt−CNT hybrid

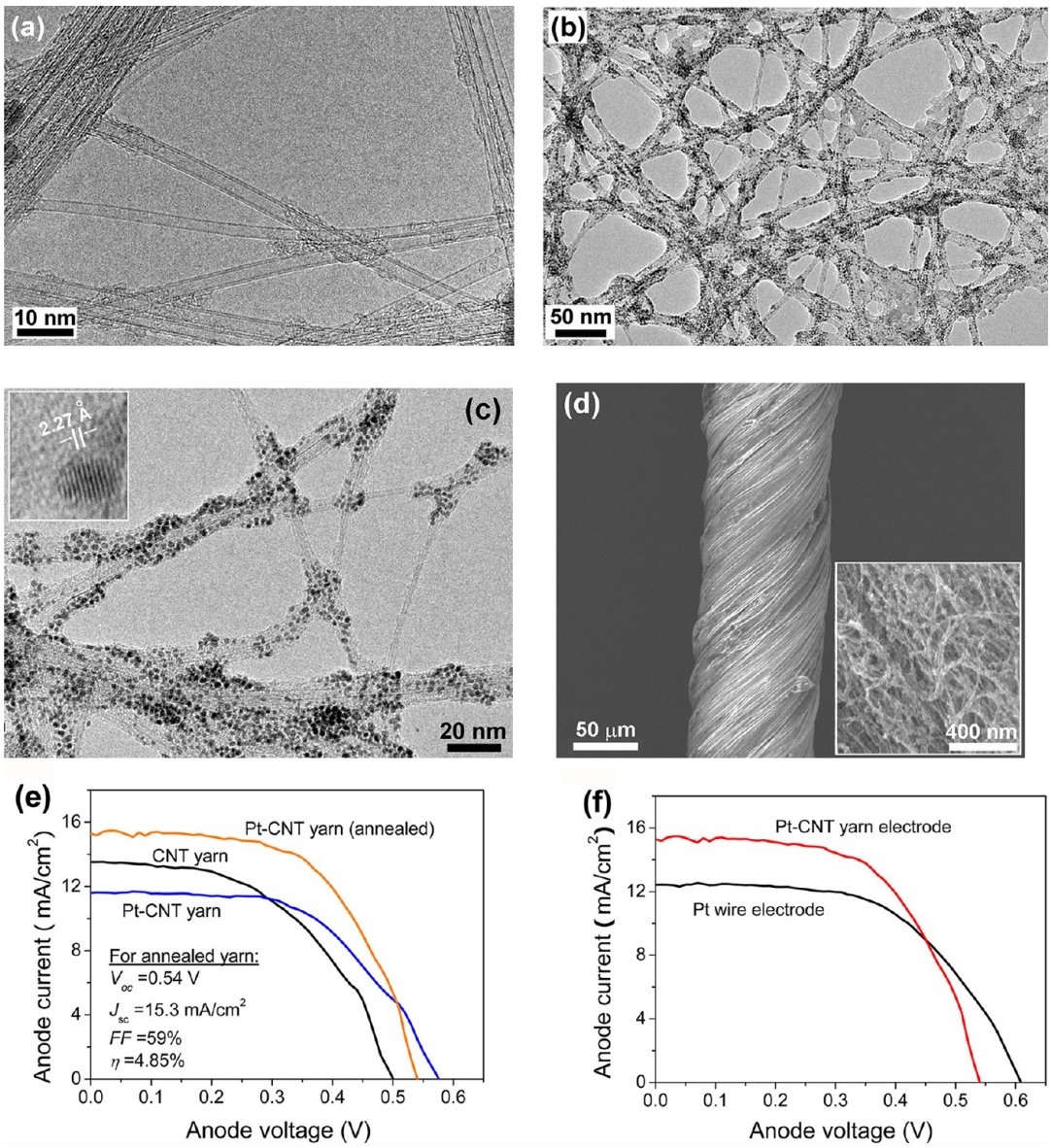

Figure 3. Hybrid Pt–CNT yarns and solar cells. (a) TEM image of a purified CNT film showing clean single-walled and double-walled nanotubes and bundles. (b) TEM image of a hybrid film after adsorption of Pt nanoparticles with a loading of 87.7 wt %. (c) Uniform 2–3 nm diameter Pt nanoparticles distributed along the CNT bundles. Inset shows a single-crystalline nanoparticle with a lattice distance of 2.27 Å. (d) SEM image of a hybrid yarn. Inset shows CNTs wrapped by Pt nanoparticles on the yarn surface. (e) *J*–*V* curves of three FSCs with a CNT yarn, a hybrid yarn, and an annealed hybrid yarn electrode, respectively. (f) Comparison of *J*–*V* curves of two FSCs with a Pt–CNT yarn (90 μm diameter, annealed) and a Pt wire electrode (100 μm diameter), respectively.

yarns contain dispersed nanoparticles throughout the yarn in a spatial distribution, rather than particle agglomerates only on the yarn surface. A close view of the hybrid yarn shows CNTs with a rough surface morphology due to attachment of Pt nanoparticles (Figure 3d). The hybrid yarn still maintains a porous structure; therefore Pt nanoparticles located within the yarn could be accessible by electrolyte infiltration and participate in redox reactions. Since the Pt nanoparticles were made in a solution process and are physically attracted to CNTs, we carried out thermal annealing on the hybrid yarns at 600 °C for 30 min in a nitrogen atmosphere, in order to clean the nanoparticle–CNT interface so that mutual interactions between the hybrid components were enhanced. A previous study showed that a strong electronic interaction exists in various nanoparticle–CNT hybrid systems. For example, fast and efficient charge transfer from semiconducting quantum dots to CNTs occurs under light excitation.[23,24] Nanoparticles within an annealed CNT yarn may grow to larger size particles since our TEM characterization on thin Pt–CNT hybrid films shows that some nanoparticles in localized regions have merged to form larger (5–20 nm) particles. Figure 3e compares the *J*–*V* characteristics of three FSCs with a pure CNT yarn, a Pt-adsorbed CNT yarn without further treatment, and

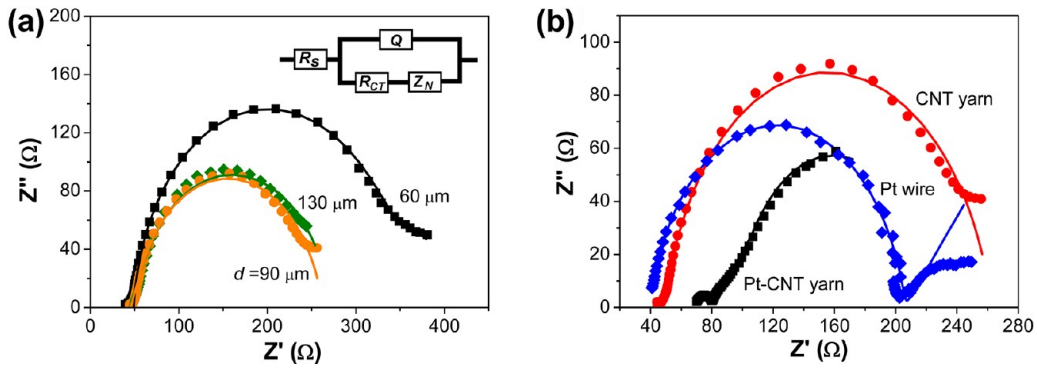

Figure 4. EIS measurements and catalytic activity. (a) EIS curves of CNT yarns with diameter (*d*) of 60, 90, and 130 μm, respectively. Inset shows the equivalent circuit containing a series resistance (R_s), a constant phase element (Q), charge transfer resistance (R_{CT}), and Nernst diffusion resistance (Z_N). (b) EIS curves of a Pt wire, a pure CNT yarn, and a Pt–CNT hybrid yarn, respectively. Experimental data are plotted as separate solid squares, circles, and diamonds, while their corresponding fitting curves are plotted as continuous lines.

an annealed Pt–CNT yarn as counter electrode, respectively, with yarn diameters around 90 μm and Pt loadings (for hybrid yarns) similar to the sample shown in Figure 3b. Without thermal annealing, the Pt-adsorbed yarn results in a cell efficiency of 3.71%, which is slightly higher than the pure CNT yarn (3.38%). However, for an annealed Pt–CNT yarn the value of J_{sc} increases to 15.28 mA/cm^2, suggesting a more efficient carrier collection process possibly due to enhanced charge transfer across the Pt–CNT interfaces after moderate temperature annealing. Consequently, the cell efficiency is enhanced to 4.85% (Figure 3e), which is higher than previously reported FSCs with a CNT film (1.6%) or CNT yarn electrode (2.94%).[14,25] The thermal annealing process is effective in making high-performance Pt–CNT hybrid yarn electrodes.

To compare our Pt nanoparticle–CNT yarns with traditional Pt electrodes, we twisted a Pt wire (100 μm diameter) around a TiO_2–Ti primary electrode to make an FSC with similar configuration. The best control sample we obtained shows a slightly increased V_{oc} of 0.61 V, possibly due to the relatively lower electrode potential of Pt,[6] but a smaller J_{sc} (12.40 mA/cm^2) and a cell efficiency at the same level (4.23%) (Figure 3f). Previously reported TiO_2 nanotube array-based FSCs with Pt wire electrodes have shown a wide range of efficiencies from 2.8% to 7%, where fabrication techniques and device parameters (*e.g.*, twisting pitch) might cause fluctuations in cell performance.[1−3,26] Here, we managed to make FSCs with different electrode materials under the same conditions in order to give an appropriate evaluation. In comparison, the cell efficiency obtained from the Pt wire electrode (4.23%) is higher than that of the pure CNT yarn (3.38%) but lower than the CNT yarn adsorbed by Pt nanoparticles (4.85%). The use of Pt nanoparticles (*versus* a solid wire) has the potential to lower the weight and cost of the electrode materials. The linear density of a typical CNT yarn (90 μm) is about 0.11 mg/cm. Therefore a Pt–CNT yarn with 87.7 wt % Pt loading (as shown in Figure 3c) has a density of about 0.89 mg/cm. On the other hand, a solid 100 μm Pt wire has a linear density of 1.68 mg/cm, which is about 2 times heavier at the same length. Meanwhile, our preliminary tests reveal that the loading of Pt nanoparticles in the CNT yarn has some influence on cell efficiency. With a reduced Pt loading of 40.4 wt %, the efficiency drops to 2.25% compared to the cell with a higher loading of 87.7 wt % (4.85% efficiency) (Figure S4a), due to the reduced number of nanoparticles and Pt–electrolyte interfacial area. Furthermore, in our process, Pt nanoparticles were first adsorbed onto a CNT film and then spun into a hybrid yarn. If the nanoparticles were loaded after the CNT yarn spinning, that is, coated mainly on the surface of the yarn, the solar cell performance was not as good as the former method and the efficiency drops to 2.37% (Figure S4b). An adsorption method that ensures uniform distribution of Pt nanoparticles is important for achieving high performance.

We have carried out electrochemical impedance spectroscopy (EIS) measurements to study the catalytic activity of those yarn electrodes (see Supporting Information for experimental procedure). Figure 4a shows the Nyquist plots of pure (Pt-free) CNT yarns with different diameters. Charge-transfer resistances at the yarn–electrolyte interface (R_{CT}) can be obtained by fitting the experimental data with an equivalent circuit of each sample, which allows us to investigate the influence of yarn size on catalytic activities. The R_{CT} value of a 90 μm diameter yarn (214.8 Ω) is smaller than a 60 μm yarn (291.6 Ω), but the decrease of R_{CT} tends to saturate as the yarn diameter further increases to 130 μm (224.6 Ω). Thicker yarns have a greater number of nanotubes and, therefore, available catalytic sites; however, beyond a certain range, the activity reaches a plateau possibly because of limited electrolyte diffusion to the inner portion through the CNT network. Solar cell characteristics also show a maximum efficiency at 90 μm over a yarn diameter range of 20 to 130 μm (Figure 2f,g). A few factors related to thicker

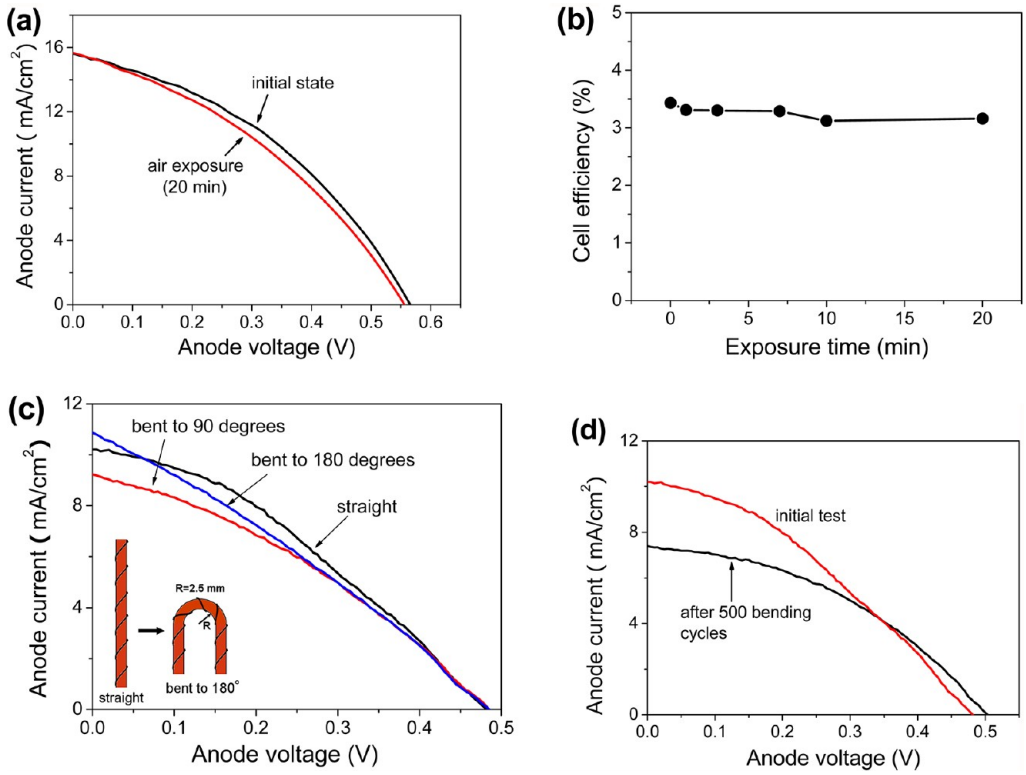

Figure 5. Stability and flexibility of FSCs with CNT yarn electrodes. (a) *J*−*V* curves of a cell with a Pt−CNT hybrid yarn electrode measured at the initial state and after being exposed to air for 20 min. (b) Calculated cell efficiencies over the period of air exposure. (c) *J*−*V* curves of an FSC with a 50 μm CNT yarn electrode tested in straight and bent forms at bending angles of 90° and 180°, respectively. The radius of curvature of the bent cell is about 2.5 mm (inset). (d) *J*−*V* curves of the FSC before and after repeated bending to 180° for 500 cycles.

yarns, such as increased blocking of incident light and reduced yarn flexibility, which is not favorable for making good contact to the primary electrode during device fabrication, may lead to a decrease in cell efficiency.

Furthermore, EIS results enable direct comparison of catalytic activities between the Pt−CNT hybrid yarn and its counterpart including pure CNT yarn and solid Pt wire. From their Nyquist plots, the reduced half-circle size of the Pt−CNT sample indicates significant improvement in the catalytic activity owing to Pt nanoparticle adsorption (Figure 4b). We found that the measured value of R_{CT} is on the order of 200 Ω for pure CNT yarns (214.8 Ω), slightly lower for solid Pt wires (166.4 Ω), and substantially reduced for thermally annealed Pt−CNT hybrid yarns (10.2 Ω), all of which have similar diameters (90 μm for two yarns and 100 μm for Pt wire). Considering their solar cell performance where the hybrid yarn results in an improved efficiency over the CNT yarn or Pt wire (Figure 3e,f), we conclude that a major underlying factor is the significantly reduced charge-transfer resistance of the Pt−CNT yarn. This mechanism is related to the electrode structure, in which a large amount of uniform Pt nanoparticles are dispersed on a highly porous CNT network, resulting in much increased interfacial area in contact with the electrolyte.

We also studied FSCs with very thin CNT yarn (*e.g.*, 20 μm in diameter) electrodes and the effect of Pt nanoparticle adsorption on solar cell characteristics. The corresponding FSC using a 20 μm yarn shows a relatively poor fill factor with only 0.49% efficiency, due to reduced yarn size and electrical conductivity. Surprisingly, Pt adsorption and subsequent annealing of this yarn lead to an overall improvement in parameters such as the J_{sc} (15.60 mA/cm^2), fill factor, and cell efficiency (3.43%) (Figure S5). Here, the series resistance of a solar cell includes the electrode (yarn) resistance and the interfacial resistance (R_{CT}). According to Figure 4b, after the solution adsorption and the annealing processes, the Pt−CNT yarn resistance increases slightly (from 45 to 65 Ω), while the R_{CT} drops significantly from about 200 down to 10 Ω. Overall, the series resistance should decrease after Pt adsorption correspondingly. Use of thinner CNT yarns has the potential to minimize light blocking in FSCs as well as to reduce material weight and device size.

Finally, the stability and mechanical flexibility of FSCs have been investigated. The porous structure of CNT yarns is ideal for liquid electrolyte infiltration by capillary effect, leading to more stable solar cell performance. To demonstrate this, we exposed an FSC with a 20 μm hybrid yarn in air and monitored its *J*−*V* characteristics for a period of 20 min, during which only

a modest decrease of cell efficiency from 3.43% to 3.16% was detected (Figure 5a). Although there was continuous electrolyte evaporation during exposure, the CNT yarn and TiO_2 nanotube arrays could retain a certain amount of solution within the pores to keep the cell working and avoid rapid degradation (Figure 5b). In contrast, the efficiency of an FSC cell with a Pt wire electrode (without encapsulation) quickly dropped to less than 0.5% in a few minutes when exposed to air. Certainly, long-term stability still necessitates appropriate encapsulation of FSCs. From a mechanical aspect, CNT yarn-incorporated FSCs are indeed flexible devices and can be curled to large angles with small fluctuation. An FSC with a 50 μm diameter yarn showed a stable V_{oc} and slightly changing J_{sc} values at bending angles up to 180° (Figure 5c). At the bent state, the 1.5 cm long fiber was curved into a "U" shape with a curvature radius of 2.5 mm (inset of Figure 5c). The flexibility of thin CNT yarns is critical for maintaining good contact with the primary electrode during large angle deformation. The cell efficiency is also stable (1.5% to 1.7%) over repeated bending to a 180° angle for 500 cycles (Figure 5d).

CONCLUSION

We demonstrated fiber solar cells with Pt nanoparticle-adsorbed CNT yarns as porous counter electrodes, with power conversion efficiencies comparable to traditional Pt wires. This electrode structure can be extended to various hybrid systems by grafting other functional nanoparticles onto CNTs and spinning into controlled size yarns. Because of the uniform spatial distribution of Pt nanoparticles throughout the porous yarn that are accessible by electrolyte infiltration, it is possible to maintain a smaller counter electrode size but provide a large interfacial catalytic area for redox reactions. Our porous Pt–CNT hybrid yarns are promising in constructing low-cost, lightweight, fiber-shaped solar cells.

METHODS

1. Fabrication of CNT and Pt–CNT Hybrid Yarns. We first synthesized CNT films using a floating catalyst CVD process with ferrocene and xylene as the catalyst precursor and carbon source. The growth temperature was set as 1160 °C, and thin CNT films were collected downstream from a nickel foil substrate. Freestanding films with lengths of >10 cm were selected to spin continuous yarns. The films were washed in H_2O_2 (30%) for 72 h to remove amorphous carbon and then further purified in hydrochloric acid (36.5%) for 72 h at room temperature to dissolve the catalyst residue. To spin the yarn, a purified film immersed in ethanol was picked up and shrunk into a thin shred during ethanol evaporation. The two ends of this film were fixed on the rotating shafts of two electric motors and spun for five minutes at a constant speed of 27 rpm for each motor operating in opposite rotating directions.

Pt nanocrystal colloids were made by a solution process. Powders of H_2PtCl_6 were dissolved in 4 mL of ethylene glycol to prepare a solution with a concentration of 100 mM. Then, about 2.5 M NaOH was added in ethylene glycol under vigorous stirring for 30 min to reach a pH value of 13 in the solution. The reduction reaction was then performed at 130 °C for 3 h under constant stirring in a 25 mL flask. The resulting solution had a black color with Pt nanoparticle diameters of 2–3 nm.

To spin hybrid yarns, a purified CNT film was transferred to a solution of Pt nanoparticles in ethylene glycol. The initially slightly condensed film expanded into a flat thin film in ethylene glycol and was immersed in the solution to ensure uniform attachment of Pt nanoparticles on the CNT surface. Generally, the adsorption process was maintained for 24 h at room temperature. The amount of Pt nanoparticles loaded on CNTs can be adjusted by the initial solution concentration. After that, excess residue Pt nanoparticles and solvent were washed away by ethanol. The Pt-adsorbed film was then spun into a hybrid yarn using the same method as for pure CNT yarns. For thermal annealing, the hybrid yarns were placed in a nitrogen atmosphere and annealed at 600 °C for 30 min.

2. Preparation of TiO_2 Nanotube Arrays. Highly ordered TiO_2 nanotube arrays were prepared by electrochemical anodization of Ti wires at room temperature in ethylene glycol solution containing 0.25 wt % NH_4F and 2 vol % water by applying a 60 V dc potential for a predefined anodizing time. By optimizing key process parameters, we obtained 70 μm long TiO_2 nanotubes by 13.5 h anodization for making the primary electrodes in fiber solar cells. The anodization was carried out in a two-electrode electrochemical cell with a Ti wire (0.25 mm diameter, 99.9% purity) about 2–3 cm in length and a Pt foil respectively serving as the anode and the cathode. After that, the TiO_2–Ti wires were washed in ethanol to remove the electrolytes used for anodization. The anatase crystallization of TiO_2 was achieved by annealing the as-anodized samples at 500 °C under ambient air for 3 h.

3. Fabrication of Fiber Solar Cells. The device fabrication process involves the following steps. First, highly ordered TiO_2 nanotube arrays radially grown around a Ti wire were immersed in a 0.05 M $TiCl_4$ solution at 70 °C for 30 min, then rinsed with distilled water and annealed at 450 °C for 30 min. After being cooled to 80 °C, the TiO_2 nanotube arrays were immersed in a dye solution of 0.3 mM *cis*-bis(isothiocyanato)bis(2,2′-bipyridyl-4,4′-dicarboxylato)ruthenium(II) bistetrabutylammonium (N719) in alcohol for 24 h, followed by an alcohol rinse to remove excess physically adsorbed dye molecules. This resulted in a primary electrode based on a dye-adsorbed TiO_2–Ti wire. Subsequently, a CNT yarn or Pt–CNT hybrid yarn was twisted around the primary electrode with a spiral pitch of 3 mm. A liquid acetonitrile electrolyte solution containing 0.6 M 1,2-dimethyl-3-propylimidazolium bis(trifluoromethylsulfonyl)imide, 0.03 M iodine, 0.1 M guanidinium thiocyanate, and 0.5 M 4-*tert*-butylpyridine was infiltrated into the pores among the TiO_2 nanotube arrays and the porous CNT yarns. The inner Ti core and the CNT yarn were connected as the anode and cathode, respectively. Usually, we use Ti wires with original lengths of 4 cm and make active regions with CNT yarn electrodes with lengths of about 2 cm.

4. Characterization and Solar Cell Tests. SEM and TEM characterizations on CNT yarns and solar cell structures were carried out in a field-emission Hitachi S4800 and a JEM-2010. Raman spectra were collected on a Jobin Yvon LabRam HR 800 micro-Raman spectrometer with 532 nm excitation. EIS measurements of the catalytic activity of pure and hybrid CNT yarns and Pt wires were carried out in an electrochemical station (Shanghai Chenhua, CHI660C). To test a particular sample such as a 90 μm Pt–CNT yarn, two identical such yarns were immersed into the same electrolyte as that used in the fiber solar cells. The immersed active yarn length was set as 1.5 cm, and the distance between two parallel yarn electrodes was maintained as 0.3 cm. A bias potential of 5 mV was applied to the yarns, and data were acquired over a frequency range of 0.1–100 000 Hz. Other yarn or Pt wire samples were tested in the same way. Photocurrent–voltage (J–V) characteristics were obtained using a Keithley model 4200 source measure unit. The cells were illuminated by solar simulator (Oriel, 91192) under AM1.5 irradiation

(100 mW/cm^2), and the light intensity was calibrated by a Si cell. The irradiated length of the FSCs was set at 0.5 cm, which was defined by a photomask with a 0.5 cm wide slit. The irradiated area is taken as the FSC length multiplied by the diameter of the Ti wire, which is the projected area of the primary electrode.

Conflict of Interest: The authors declare no competing financial interest.

Supporting Information Available: Figures S1−S5. This material is available free of charge via the Internet at http://pubs.acs.org.

Acknowledgment. This work is supported by the National Natural Science Foundation of China (Grant No. 90922004, 20821091), National Basic Research Program of China (Grant No. 2011CB933300), and National High Technology Research and Development Program of China (Grant No. 2012AA050702). A.C. acknowledges financial support from the NSFC grant (51072005).

REFERENCES AND NOTES

1. Lv, Z.; Fu, Y.; Hou, S.; Wang, D.; Wu, H.; Zhang, C.; Chu, Z.; Zou, D. Large Size, High Efficiency Fiber-Shaped Dye-Sensitized Solar Cells. *Phys. Chem. Chem. Phys.* **2011**, *13*, 10076–10083.
2. Fu, Y.; Lv, Z.; Hou, S.; Wu, H.; Wang, D.; Zhang, C.; Chu, Z.; Cai, X.; Fan, X.; Wang, Z. L.; *et al*. Conjunction of Fiber Solar Cells with Groovy Micro-Reflectors as Highly Efficient Energy Harvesters. *Energ. Environ. Sci.* **2011**, *4*, 3379–3383.
3. Lv, Z.; Yu, J.; Wu, H.; Shang, J.; Wang, D.; Hou, S.; Fu, Y.; Wu, K.; Zou, D. Highly Efficient and Completely Flexible Fiber-Shaped Dye-Sensitized Solar Cell Based on TiO_2 Nanotube Array. *Nanoscale* **2012**, *4*, 1248–1253.
4. Zou, D.; Wang, D.; Chu, Z.; Lv, Z.; Fan, X. Fiber-Shaped Flexible Solar Cells. *Coord. Chem. Rev.* **2010**, *254*, 1169–1178.
5. Huang, S.; Guo, X.; Huang, X.; Zhang, Q.; Sun, H.; Li, D.; Luo, Y.; Meng, Q. Highly Efficient Fibrous Dye-Sensitized Solar Cells Based on TiO_2 Nanotube Arrays. *Nanotechnology* **2011**, *22*, 315402.
6. Hagfeldt, A.; Boschloo, G.; Sun, L.; Kloo, L.; Pettersson, H. Dye-Sensitized Solar Cells. *Chem. Rev.* **2010**, *110*, 6595–6663.
7. Zhang, W.; Minett, A. I.; Gao, M.; Zhao, J.; Razal, J. M.; Wallace, G. G.; Romeo, T.; Chen, J. Integrated High-Efficiency Pt/Carbon Nanotube Arrays for PEM Fuel Cells. *Adv. Energy Mater.* **2011**, *1*, 671–677.
8. Wen, Z.; Wang, Q.; Li, J. Template Synthesis of Aligned Carbon Nanotube Arrays Using Glucose as a Carbon Source: Pt Decoration of Inner and Outer Nanotube Surfaces for Fuel-Cell Catalysts. *Adv. Funct. Mater.* **2008**, *18*, 959–964.
9. Tian, Z. Q.; Lim, S. H.; Poh, C. K.; Tang, Z.; Xia, Z.; Luo, Z.; Shen, P. K.; Chua, D.; Feng, Y. P.; Shen, Z.; *et al*. A Highly Order-Structured Membrane Electrode Assembly with Vertically Aligned Carbon Nanotubes for Ultra-Low Pt Loading PEM Fuel Cells. *Adv. Energy Mater.* **2011**, *1*, 1205–1214.
10. Fu, Y.; Lv, Z.; Hou, S.; Wu, H.; Wang, D.; Zhang, C.; Zou, D. TCO-Free, Flexible, And Bifacial Dye-Sensitized Solar Cell Based on Low-Cost Metal Wires. *Adv. Energy Mater.* **2012**, *2*, 37–41.
11. Hou, S.; Lv, Z.; Wu, H.; Cai, X.; Chu, Z.; Yiliguma; Zou, D. Flexible Conductive Threads for Wearable Dye-Sensitized Solar Cells. *J. Mater. Chem.* **2012**, *22*, 6549–6552.
12. Cai, X.; Hou, S.; Wu, H.; Lv, Z.; Fu, Y.; Wang, D.; Zhang, C.; Kafafy, H.; Chu, Z.; Zou, D. All-Carbon Electrode-Based Fiber-Shaped Dye-Sensitized Solar Cells. *Phys. Chem. Chem. Phys.* **2012**, *14*, 125–130.
13. Hou, S.; Cai, X.; Fu, Y.; Lv, Z.; Wang, D.; Wu, H.; Zhang, C.; Chu, Z.; Zou, D. Transparent Conductive Oxide-less, Flexible, and Highly Efficient Dye-Sensitized Solar Cells with Commercialized Carbon Fiber as the Counter Electrode. *J. Mater. Chem.* **2011**, *21*, 13776–13779.
14. Chen, T.; Qiu, L.; Cai, Z.; Gong, F.; Yang, Z.; Wang, Z.; Peng, H. Intertwined Aligned Carbon Nanotube Fiber Based Dye-Sensitized Solar Cells. *Nano Lett.* **2012**, *12*, 2568–2572.
15. Huang, S.; Zhang, Q.; Huang, X.; Guo, X.; Deng, M.; Li, D.; Luo, Y.; Shen, Q.; Toyoda, T.; Meng, Q. Fibrous CdS/CdSe Quantum Dot Co-Sensitized Solar Cells Based on Ordered TiO_2 Nanotube Arrays. *Nanotechnology* **2010**, *21*, 375201.
16. Mathew, A.; Rao, G. M.; Munichandraiah, N. Dye Sensitized Solar Cell Based on Platinum Decorated Multiwall Carbon Nanotubes as Catalytic Layer on the Counter Electrode. *Mater. Res. Bull.* **2011**, *46*, 2045–2049.
17. Wang, H. Y.; Wang, F. M.; Wang, Y. Y.; Wan, C. C.; Hwang, B. J.; Santhanam, R.; Rick, J. Electrochemical Formation of Pt Nanoparticles on Multiwalled Carbon Nanotubes: Useful for Fabricating Electrodes for Use in Dye-Sensitized Solar Cells. *J. Phys. Chem. C* **2011**, *115*, 8439–8446.
18. Xiao, Y.; Wu, J.; Yue, G.; Lin, J.; Huang, M.; Lan, Z. Low Temperature Preparation of a High Performance Pt/SWCNT Counter Electrode for Flexible Dye-Sensitized Solar Cells. *Electrochim. Acta* **2011**, *56*, 8545–8550.
19. Lima, M. D.; Fang, S.; Lepro, X.; Lewis, C.; Ovalle-Robles, R.; Carretero-Gonzalez, J.; Castillo-Martinez, E.; Kozlov, M. E.; Oh, J.; Rawat, N.; Haines, C. S.; *et al*. Biscrolling Nanotube Sheets and Functional Guests into Yarns. *Science* **2011**, *331*, 51–55.
20. Lin, Z.; Chu, H.; Shen, Y.; Wei, L.; Liu, H.; Li, Y. Rational Preparation of Faceted Platinum Nanocrystals Supported on Carbon Nanotubes with Remarkably Enhanced Catalytic Performance. *Chem. Commun.* **2009**, 7167–7169.
21. Li, Z.; Jia, Y.; Wei, J.; Wang, K.; Shu, Q.; Gui, X.; Zhu, H.; Cao, A.; Wu, D. Large Area, Highly Transparent Carbon Nanotube Spiderwebs for Energy Harvesting. *J. Mater. Chem.* **2010**, *20*, 7236–7240.
22. Trancik, J. E.; Barton, S. C.; Hone, J. Transparent and Catalytic Carbon Nanotube Films. *Nano Lett.* **2008**, *8*, 982–987.
23. Li, X.; Jia, Y.; Wei, J.; Zhu, H.; Wang, K.; Wu, D.; Cao, A. Solar Cells and Light Sensors Based on Nanoparticle-Grafted Carbon Nanotube Films. *ACS Nano* **2010**, *4*, 2142–2148.
24. Hu, L. B.; Zhao, Y. L.; Ryu, K.; Zhou, C.; Stoddart, J. F.; Gruner, G. Light-Induced Charge Transfer in Pyrene/CdSe-SWNT Hybrids. *Adv. Mater.* **2008**, *20*, 939–946.
25. Zhang, S.; Ji, C.; Bian, Z.; Liu, R.; Xia, X.; Yu, D.; Zhang, L.; Huang, C.; Cao, A. Single-Wire Dye-Sensitized Solar Cells Wrapped by Carbon Nanotube Film Electrodes. *Nano Lett.* **2011**, *11*, 3383–3387.
26. Liu, Z.; Misra, M. Dye-Sensitized Photovoltaic Wires Using Highly Ordered TiO_2 Nanotube Arrays. *ACS Nano* **2010**, *4*, 2196–2200.